Fate of exceptional points under interactions: Reduction of topological classifications

Tsuneya Yoshida and Yasuhiro Hatsugai

Phys. Rev. B **107**, 075118 — Published 8 February 2023

DOI: 10.1103/PhysRevB.107.075118

Fate of exceptional points under interactions: Reduction of topological classifications

Tsuneya Yoshida
Department of Physics, Kyoto University, Kyoto 606-8502, Japan

Yasuhiro Hatsugai
Department of Physics, University of Tsukuba, Ibaraki 305-8571, Japan

(Dated: January 20, 2023)

Despite recent extensive studies of the non-Hermitian topology, understanding interaction effects is left as a crucial question. In this paper, we address interaction effects on exceptional points which are protected by the non-trivial point-gap topology unique to non-Hermitian systems. Our analysis in a two-dimensional parameter space elucidates the existence of exceptional points and symmetry-protected exceptional rings fragile against interactions; they are topologically protected only in non-interacting cases. This fragility of exceptional points and symmetry-protected exceptional rings arises from the reduction of non-Hermitian topological classifications, which is elucidated by introducing topological invariants of the second-quantized Hamiltonian for both non-interacting and interacting cases. These topological invariants are also available to analyze the reduction phenomena of gapped systems. The above results strongly suggest similar reduction phenomena of exceptional points in generic cases and open up a new direction of research in the non-Hermitian topology.

I. INTRODUCTION

Extensive efforts have been devoted to understanding effects of interactions on topological insulators/superconductors. In particular, it has turned out that interplay between the topology and interactions triggers off exotic phenomena such as the emergence of fractional topological insulators[1–8] and topological Mott insulators[9]. Furthermore, it has been elucidated that interactions change the topological classification of free fermions[10–12] which provides systematic understanding of topological states and serves as the corner stone of the material searching. For instance, interactions change the $\mathbb{Z}$-classification to the $\mathbb{Z}_8$-classification for one-dimensional topological superconductors with time-reversal symmetry[13]. This fact indicates that the number of possible topological states is reduced by interactions; there exist an infinite number of topologically distinct states in non-interacting cases while there exist four topologically distinct states in interacting cases. Further extensive works have elucidated the ubiquity of such reduction of topological classifications[14–37]. Namely, the reduction phenomena occur for arbitrary dimensions and symmetry classes. In addition, they occur even in parameter spaces[38].

In parallel with the above significant developments, in these years, a topological aspect of non-Hermitian systems attracts as one of hot topics in condensed matter physics[39–52]. For such systems, extensive works of the non-interacting non-Hermitian topology have discovered a variety of novel phenomena induced by the point-gap topology unique to non-Hermitian systems, such as non-Hermitian skin effects which result in extreme sensitivity to the presence/absence of boundaries[53–5960,61]. Furthermore, the non-Hermiticity induces a new type of topological degeneracies dubbed exceptional points (EPs) which are protected by the point-gap topology[62–67]. This new type of topological degeneracies is further enriched by symmetry, which results in the emergence of symmetry-protected exceptional rings (SPERs) and symmetry-protected exceptional surfaces in two and three dimensions, respectively[68–74]. The EPs and their symmetry-protected variants in non-interacting systems attract interdisciplinary interests because they are reported for a wide variety of systems[60,65–67,75–81].

The above two progresses lead us the following issues to be addressed; effects of interactions on the non-Hermitian topology. Although several works addressed this issue[82–103], fate of EPs under interactions remains highly crucial question. The significance of this question is further enhanced by recent experimental progresses in cold atoms[104–106] and quantum circuits[107].

We hereby analyze effects of interactions on an EP and an SPER in a two-dimensional parameter space which are protected by symmetry. In particular, we elucidate that interactions may destroy the EP and the SPER without breaking relevant symmetry. The above fragility of EPs against interactions arises from the reduction of the non-Hermitian topological classification, which is obtained by comparing topological invariants of the second-quantized Hamiltonian for both non-interacting and interacting cases. Specifically, our analysis elucidates that the reduction $\mathbb{Z}^{(N+P'+1)/2} \to \mathbb{Z}$ ($\mathbb{Z} \to \mathbb{Z}_2$) results in the fragility of EPs (SPERs) for systems with charge U(1) symmetry and spin-parity symmetry (chiral symmetry). Here, we have focused on the Fock space with the particle number N. For even (odd) N, P' takes ± 1 (0).

The above topological invariants are also applicable to the reduction for gapped systems[92,102]. For gapped systems with charge U(1) symmetry and spin-parity symmetry, our topological invariants indicate the reduction of one-dimensional point-gap topology: $\mathbb{Z}^{(N+P'+1)/2} \to \mathbb{Z}$. For gapped systems with chiral symmetry, our topological invariants indicate the reduction of zero-dimensional

point-gap topology: $\mathbb{Z} \to \mathbb{Z}_2$.

The rest of this paper is organized as follows. Section II is devoted to clarifying the fragility of EPs against interactions in systems with charge U(1) symmetry and spin-parity symmetry. Section III elucidates the fragility of SPERs with chiral symmetry. In Sec. IV, a brief summary is provided. In Appendix A, we count the number of the subspaces for a given Fock space. In Appendix B, we demonstrate that there also exist EPs robust against interactions. In Appendices C and D, we address the reduction phenomena for gapped systems[92,102] by computing the above topological invariants.

II. EXCEPTIONAL POINTS WITH CHARGE U(1) SYMMETRY AND SPIN-PARITY SYMMETRY

There exist EPs protected by the point-gap topology only when the second-quantized Hamiltonian is quadratic. In order to see this, let us analyze interaction effects on EPs for the two-dimensional parameter space in the presence of charge U(1) symmetry and spin-parity symmetry. The Hamiltonian reads,

$$\hat{H} = \hat{H}_0 + \hat{H}_{\rm int}, \tag{1a}$$

$$\hat{H}_0 = \hat{\Psi}^\dagger_\alpha h_{\alpha\beta}(x,y)\hat{\Psi}_\beta. \tag{1b}$$

Here, summation is assumed over the repeated indices. The first-quantized Hamiltonian is denoted by $h(x,y)$. Real variables x and y describe the two-dimensional parameter space. Operator $\hat{\Psi}^\dagger$ ($\hat{\Psi}$) denotes a set of creation operators $\hat{c}^\dagger_\alpha$ (annihilation operators $\hat{c}_\alpha$) of fermions. The subscripts α and β label the internal degrees of freedom such as orbital and spin. Here, one might consider that the above setup is somewhat artificial. However, EPs in such a parameter space have been reported for quantum circuits[79,80].

In this section, we consider a system of fermions with spin-1/2 whose Hamiltonian preserves charge U(1) symmetry and spin-parity symmetry;

$$[\hat{H}, \hat{N}]_{\rm c} = 0, \tag{2a}$$

$$[\hat{H}, e^{i\pi\hat{S}_z}]_{\rm c} = 0, \tag{2b}$$

with $\hat{N} = \hat{N}_\uparrow + \hat{N}_\downarrow$ and $\hat{S}_z = (\hat{N}_\uparrow - \hat{N}_\downarrow)/2$. Here $\hat{N}_\sigma$ denotes the operator of the total number of fermions in spin-state $\sigma =\uparrow,\downarrow$. The commutation relation denoted by square brackets $[\hat{A},\hat{B}]_{\rm c} := \hat{A}\hat{B} - \hat{B}\hat{A}$. The above equations indicates that the second-quantized Hamiltonian $\hat{H}$ can be block-diagonalized with respect to $\hat{N}$ and $\hat{P} = (-1)^{\hat{N}_\uparrow} = e^{i\pi\hat{N}/2}e^{i\pi\hat{S}_z}$. We denote eigenvalues of $\hat{N}$, $\hat{S}_z$, $\hat{N}_\sigma$ and $\hat{P}$ by N, S_z, N_σ and P, respectively.

In the reset of this section, we introduce topological invariants and demonstrate the presence of EPs which are fragile against interactions.

A. Topological invariants

For the Fock space with $[N,P]$, the number $(N+P'+1)/2$ of $\mathbb{Z}$-invariants are introduced in the non-interacting cases, while the number of $\mathbb{Z}$-invariants is reduced to one in the presence of interactions. Here, P' takes P (0) for even (odd) N. This fact indicates the reduction of the topological classification of $\hat{H}$: $\mathbb{Z}^{(N+P'+1)/2} \to \mathbb{Z}$ (for application to gapped systems, see Appendix C). In other words, there exist EPs which are destroyed by interactions without breaking relevant symmetry. The key ingredient is the additional symmetry imposed on the quadratic Hamiltonian $\hat{H}_0$ [see Eq. (4)].

1. *Non-interacting case*

In the presence of the spin-parity symmetry (2b), the number $(N+P'+1)/2$ of $\mathbb{Z}$-invariants can be introduced when the second-quantized Hamiltonian is quadratic.

Firstly, we note that the spin-parity symmetry imposes the following constraint on the first-quantized Hamiltonian

$$[h, s_z]_{\rm c} = 0, \tag{3}$$

with s_z being the z-component of the first-quantized spin operator. This commutation relation can be seen by noting the relation $e^{i\pi\hat{S}_z}\hat{\Psi}^\dagger_\alpha e^{-i\pi\hat{S}_z} = e^{i\pi(s_z)_{\alpha\beta}}\hat{\Psi}^\dagger_\beta$. The above constraint indicates that at the non-interacting level, the second-quantized Hamiltonian $\hat{H}_0$ satisfies

$$[\hat{H}_0, \hat{S}_z]_{\rm c} = 0, \tag{4}$$

meaning that the $\hat{H}_0$ can be block-diagonalized with respect to $\hat{S}_z$.

Thus, the Fock space with $[N,P]$ can be divided into subspaces with $(N_\uparrow, N_\downarrow)$. For each subspace with $(N_\uparrow, N_\downarrow)$, the following winding number can be introduced

$$W_{(N_\uparrow,N_\downarrow)} = \oint \frac{d\boldsymbol{\lambda}}{2\pi i}\cdot \boldsymbol{\partial}_{\boldsymbol{\lambda}} \log\det[\hat{H}_{(N_\uparrow,N_\downarrow)}(\boldsymbol{\lambda}) - E_{\rm ref}\mathbb{1}], \tag{5}$$

with the block-diagonalized Hamiltonian $\hat{H}_{(N_\uparrow,N_\downarrow)}$, the reference energy $E_{\rm ref} \in \mathbb{C}$, and the identity matrix $\mathbb{1}$. The integral is taken over a closed path parameterized by $\boldsymbol{\lambda} = (x,y)$ in the two-dimensional parameter space. Here, we have supposed that along the path, the point-gap opens at the reference energy $E_{\rm ref}$; $\det[\hat{H}_{(N_\uparrow,N_\downarrow)}(\boldsymbol{\lambda}) - E_{\rm ref}\mathbb{1}] \neq 0$ holds for $\boldsymbol{\lambda}$ parameterizing the path. Here, we note that for a given set of $[N,P]$, the number $(N+P'+1)/2$ of the sets $(N_\uparrow, N_\downarrow)$ are allowed where P' takes P (0) for even (odd) N. The detailed derivation is provided in Appendix A.

Therefore, it is concluded that the number $(N+P'+1)/2$ of $\mathbb{Z}$-invariants are introduced in the non-interacting cases.

2. *Interacting case*

For correlated systems, the second-quantized Hamiltonian can be block-diagonalized not with $\hat{S}_z$ but with $\hat{P} = (-1)^{\hat{N}_\uparrow}$ due to spin-parity symmetry.

Thus, the point-gap topology is characterized by

$$W_{[N,P]} = \oint \frac{d\boldsymbol{\lambda}}{2\pi i} \cdot \boldsymbol{\partial}_{\boldsymbol{\lambda}} \log \det[\hat{H}_{[N,P]}(\boldsymbol{\lambda}) - E_{\rm ref}\mathbb{1}]. \quad (6)$$

Here, $\hat{H}_{[N,P]}(\boldsymbol{\lambda})$ denotes the second-quantized Hamiltonian for the Fock space with $[N, P]$.

In the non-interacting case, the above winding numbers satisfy

$$W_{[N,P]} = \sum_{(N_\uparrow,N_\downarrow)}{}' W_{(N_\uparrow,N_\downarrow)}, \quad (7)$$

where the summation is taken over sets of $N_\uparrow$ and $N_\downarrow$ satisfying $N_\uparrow + N_\downarrow = N$ and $(-1)^{N_\uparrow} = P$ for given N and P.

Equation (7) indicates that for the Fock space with $[N, P]$, the point-gap topological states form the $\mathbb{Z}^{(N+P'+1)/2}$ group in the non-interacting case while the point-gap topological states form its subgroup $\mathbb{Z}$ in correlated cases In particular, it indicates that interactions may destroy EPs without breaking charge U(1) symmetry and spin-parity symmetry if they are characterized by vanishing $W_{[N,P]}$ and finite $W_{(N_\uparrow,N_\downarrow)}$.

B. Analysis of a toy model

EPs can be fragile against interactions due to the reduction of the non-Hermitian topological classification for systems with charge U(1) symmetry and spin-parity symmetry. In order to demonstrate this fact, let us analyze a three-orbital system described by the second-quantized Hamiltonian (1) with $\hat{\Psi} = (\hat{c}_{a\uparrow}, \hat{c}_{b\uparrow}, \hat{c}_{c\uparrow}, \hat{c}_{a\downarrow}, \hat{c}_{b\downarrow}, \hat{c}_{c\downarrow})^T$,

$$h(x,y) = \left(\begin{array}{ccc|ccc} 0 & x+iy & 0 & & & \\ 1 & 0 & 0 & & & \\ 0 & 0 & 0 & & & \\ \hline & & & 0 & 1 & 0 \\ & & & x+is_\downarrow y & 0 & 0 \\ & & & 0 & 0 & 0 \end{array}\right), \quad (8)$$

and

$$\hat{H}_{\rm int} = iV[(\hat{S}_a^+ + \hat{S}_b^+)\hat{S}_c^+ + {\rm h.c.}]. \quad (9)$$

Here, a fermion in orbital $l = a, b, c$ and spin-state $\sigma = \uparrow, \downarrow$ is created (annihilated) by applying operator $\hat{c}_{l\sigma}^\dagger$ ($\hat{c}_{l\sigma}$). The parameter $s_\downarrow$ takes 1 or -1. Unless otherwise noted, we set $s_\downarrow = -1$ in the main text. Operator $\hat{S}_l^+$ ($\hat{S}_l^-$) is defined as $\hat{S}_l^+ = c_{l\uparrow}^\dagger c_{l\downarrow}$ ($\hat{S}_l^- = c_{l\downarrow}^\dagger c_{l\uparrow}$). The prefactor V is real. The above Hamiltonian satisfies $[\hat{H}, \hat{n}_{c\sigma}]_{\rm c} = 0$ for $\sigma = \uparrow, \downarrow$, and thus, we suppose that[108] a fermion occupies orbital c. In this section, we focus on the Fock space with $[N, P] = [2, 1]$ because there is no topologically protected EPs in the other subspace[109] with $N = 2$.

Let us start with the non-interacting case. For the Fock space specified by $[N, P] = [2, 1]$, the second-quantized Hamiltonian $\hat{H}_{0[2,1]}$ is written as

$$\hat{H}_{0[2,1]} = \left(\begin{array}{c|c} \hat{H}_{0(2,0)} & 0 \\ \hline 0 & \hat{H}_{0(0,2)} \end{array}\right), \quad (10a)$$

with

$$\hat{H}_{0(2,0)} = \begin{pmatrix} 0 & x+iy \\ 1 & 0 \end{pmatrix}, \quad (10b)$$

$$\hat{H}_{0(0,2)} = \begin{pmatrix} 0 & 1 \\ x+is_\downarrow y & 0 \end{pmatrix}. \quad (10c)$$

Here we have chosen the basis as

$$(c_{a\uparrow}^\dagger c_{c\uparrow}^\dagger|0\rangle, c_{b\uparrow}^\dagger c_{c\uparrow}^\dagger|0\rangle, c_{a\downarrow}^\dagger c_{c\downarrow}^\dagger|0\rangle, c_{b\downarrow}^\dagger c_{c\downarrow}^\dagger|0\rangle). \quad (11)$$

The matrix $\hat{H}_{0(2,0)}$ [$\hat{H}_{0(0,2)}$] is the Hamiltonian for the subspace with $(N_\uparrow, N_\downarrow) = (2, 0)$ [$(0, 2)$]. The above equation is consistent with the fact that the non-interacting Hamiltonian $\hat{H}_0$ can be block-diagonalized with respect to $\hat{S}_z$ in the presence of spin-parity symmetry [see Eq. (4)].

The Hamiltonian $\hat{H}_{[2,1]}$ exhibits EPs for $V = 0$, which can be seen by diagonalizing $\hat{H}_{0(2,0)}$ and $\hat{H}_{0(0,2)}$. Figures 1(a) and 1(b) display eigenvalues of $\hat{H}_{0[2,1]}$ against x and y. In these figures, EPs emerge at zero energy $E = 0$ and $(x, y) = (0, 0)$ which are denoted by red dots. The point-gap topology protecting these EPs

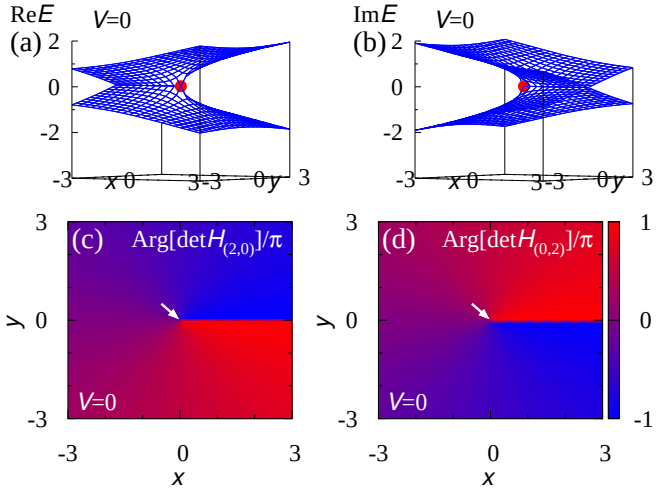

FIG. 1. (a) [(b)] The real- [imaginary-] part of eigenvalues of $\hat{H}_{[2,1]}$ for $V = 0$. (c) [(d)] The argument of $\det\hat{H}_{0(2,0)}$ [$\det\hat{H}_{0(0,2)}$]. We recall that $\hat{H}_{[N,P]}$ and $\hat{H}_{(N_\uparrow,N_\downarrow)}$ denote the Hamiltonian for the Fock space with $[N, P]$ and $(N_\uparrow, N_\downarrow)$. The data are obtained for $s_\downarrow = -1$.

is characterized by the winding numbers. For computation of $W_{(2,0)}$ and $W_{(0,2)}$, we plot $\det[\hat{H}_{(N_\uparrow,N_\downarrow)}]$ for $(N_\uparrow, N_\downarrow) = (2,0)$ and $(0,2)$ in Figs. 1(c) and 1(d), respectively. From these figure, we can extract the winding numbers $\left(W_{(2,0)}, W_{(0,2)}\right) = (1,-1)$ for $E_{\rm ref} = 0$ computed along a path enclosing the origin $(x,y) = (0,0)$. Here, the path is taken so that it winds the origin in the counterclockwise direction. Therefore, the EPs [see Figs. 1(a) and 1(b)] are robust against perturbations at the non-interacting level because they are protected by the non-trivial point-gap topology.

In the presence of interactions, however, the above EPs are no longer protected by the topology, implying that they can be destroyed by interactions. This is because the subspaces with $(N_\uparrow, N_\downarrow) = (2,0)$ and $(0,2)$ are unified in the presence of interactions.

Specifically, Eq. (7) elucidates that the point-gap topology is trivial in the presence of interactions; $W_{[2,1]} = W_{(2,0)} + W_{(0,2)} = 0$ for $E_{\rm ref} = 0$. Correspondingly, introducing the interaction (9) destroys EPs. For the Fock space with $[N,P] = [2,1]$, the second-quantized Hamiltonian is written as

$$\hat{H}_{[2,1]} = \hat{H}_{0[2,1]} + \hat{H}_{{\rm int}[2,1]}, \tag{12a}$$

$$\hat{H}_{{\rm int}[2,1]} = iV \left(\begin{array}{cc|cc} 0 & 0 & 1 & 0 \\ 0 & 0 & 0 & 1 \\ \hline 1 & 0 & 0 & 0 \\ 0 & 1 & 0 & 0 \end{array}\right), \tag{12b}$$

with the basis defined in Eq. (11). Figures 2 displays eigenvalues of $\hat{H}_{[2,1]}$ for $V = 1$. As observed in this figure, EPs are destroyed by interaction V which mixes the subspaces with $(N_\uparrow, N_\downarrow) = (2,0)$ and $(0,2)$.

Putting the above results [Figs. 1 and 2 and Eq. (7)] together, we end up with the conclusion that the reduction $\mathbb{Z}^2 \to \mathbb{Z}$ results in the fragility of EPs against interactions for the Fock space with $[N,P] = [2,1]$.

We finish this section with two remarks. Firstly, we note that if the winding number $W_{[N,P]}$ is finite, the EPs are robust against interactions, which can be seen in the case for $s_\downarrow = 1$ (see Appendix B).

Secondly, we point out that for the Fock space with $[N,P] = [2,1]$, the winding numbers can be analytically computed along the path specified by $x^2 + y^2 = 1$. Along this path the Hamiltonian is written as

$$\hat{H}_{[2,1]} = \left(\begin{array}{cc|cc} 0 & e^{i\theta} & iV & 0 \\ 1 & 0 & 0 & iV \\ \hline iV & 0 & 0 & 1 \\ 0 & iV & e^{is_\downarrow\theta} & 0 \end{array}\right), \tag{13}$$

with $(x,y) = (\cos\theta, \sin\theta)$ and $0 \le \theta < 2\pi$. Here, we have chosen the basis (11). Diagonalizing the above Hamiltonian, we have eigenvalues[110] for $s_\downarrow = -1$

$$E_{{\rm p}\pm}(\theta) = \left[\cos\frac{\theta}{2} \pm i\sqrt{\sin^2\frac{\theta}{2} + V^2}\right], \tag{14a}$$

$$E_{{\rm m}\pm}(\theta) = -\left[\cos\frac{\theta}{2} \pm i\sqrt{\sin^2\frac{\theta}{2} + V^2}\right]. \tag{14b}$$

For $V = 0$, eigenvalues for the subspace with $(N_\uparrow, N_\downarrow) = (2,0)$ are given by $(E_{\rm p+}, E_{\rm m+}) = (e^{i\frac{\theta}{2}}, -e^{i\frac{\theta}{2}})$, which indicates $W_{(2,0)} = 1$ for $E_{\rm ref} = 0$. In a simiar way, we obtain $W_{(0,2)} = -1$ along the loop. For $V > 0$, Eq. (14) indicates that the imaginary-part of all eigenvalues are finite for $0 \le \theta < 2\pi$. This fact results in $W_{[2,1]} = 0$ because no eigenvalue winds the origin. The above analysis is consistent with Eq. (7).

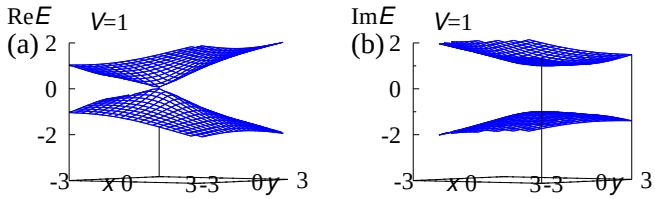

FIG. 2. (a) [(b)] The real- [imaginary-] part of eigenvalues of $\hat{H}_{[2,1]}$ for $V = 1$.

III. SYMMETRY-PROTECTED EXCEPTIONAL RING WITH CHIRAL SYMMETRY

As is the case of EPs, there exist SPERs protected by the point-gap topology only when the Hamiltonian is quadratic. In order to see this, let us analyze interaction effects on SPERs for the two-dimensional parameter space in the presence of chiral symmetry. Consider the Hamiltonian (1) preserving chiral symmetry

$$[\hat{H}, \hat{\Xi}]_{\rm c} = 0, \tag{15}$$

with anti-unitary operator $\hat{\Xi}$ which is a product of time-reversal and charge conjugation operators. In the reset of this section, we introduce zero-dimensional topological invariants and demonstrate the presence of SPERs which are fragile against interactions.

A. Topological invariants

For a given Fock space, a zero-dimensional $\mathbb{Z}$- ($\mathbb{Z}_2$-) invariant can be introduced in non-interacting (interacting) cases. This fact indicates the reduction of the topological classification of $\hat{H}$: $\mathbb{Z} \to \mathbb{Z}_2$ (for application to a gapped system, see Appendix D). In other words, there exist SPERs destroyed by interactions without breaking chiral symmetry. As is the case of Sec. II, the key ingredient is

an additional constraint imposed only on the quadratic Hamiltonian $\hat{H}_0$ [see Eq. (18a)].

We also note that Eq. (21) is essential for the above reduction.

1. Non-interacting case

In the presence of chiral symmetry, a zero-dimensional $\mathbb{Z}$-invariant can be introduced when the second-quantized Hamiltonian is quadratic.

Firstly, we note that the chiral symmetry (15) imposes the following constraint on the first-quantized Hamiltonian

$$\xi h^\dagger \xi = -h, \tag{16}$$

with unitary matrix ξ satisfying [111] $\xi^2 = \mathbb{1}$. Here, we have considered that h is a traceless matrix. We note that the chiral symmetric $\hat{H}_0$ may include $i\gamma_\alpha\left(\hat{n}_\alpha - \frac{1}{2}\right)$ with $\gamma_\alpha \in \mathbb{R}$ and $\hat{n}_\alpha = \hat{c}_\alpha^\dagger \hat{c}_\alpha$. However, this fact does not affect the following argument. Equation (16) can be seen by noting the relation

$$\hat{\Xi}\hat{\Psi}_\alpha^\dagger \hat{\Xi}^{-1} = \xi_{\alpha\beta}\hat{\Psi}_\beta. \tag{17}$$

Summation is assumed over repeated indices.

As proved below, Eq. (16) results in the following constraint on $\hat{H}_0$:

$$\hat{H}_0 = -\hat{\Gamma}\hat{H}_0^\dagger \hat{\Gamma}, \tag{18a}$$

with

$$\hat{\Gamma} = (-1)^{\hat{N}_-}, \tag{18b}$$

$$\hat{N}_- = \Psi^\dagger \left(\frac{\mathbb{1} - \xi}{2}\right)\Psi. \tag{18c}$$

Equation (18a) can be proven as follows. Firstly, we rewrite Eq. (16) as

$$\xi h_{\rm H} \xi = -h_{\rm H}, \tag{19a}$$

$$\xi h_{\rm A} \xi = h_{\rm A}, \tag{19b}$$

where we have decomposed h into the Hermitian part $h_{\rm H}$ and the anti-Hermitian part $h_{\rm A}$. Equation (19a) indicates that applying $\hat{H}_{0{\rm H}} = \Psi^\dagger h_{\rm H}\Psi$ increases/decreases the number N_- by one [112], where N_- denotes eigenvalues of $\hat{N}_-$. Thus, $\hat{H}_{0{\rm H}}$ anti-commutes with $\hat{\Gamma} = (-1)^{\hat{N}_-}$. Equation (19b) indicates that $\hat{H}_{0{\rm A}} = \Psi^\dagger h_{\rm A}\Psi$ commutes with $\hat{\Gamma}$. Noting the relation $\hat{H}_0 = \hat{H}_{0{\rm H}} + \hat{H}_{0{\rm A}}$, we obtain Eq. (18a).

Equation (18a) allows us to define the zero-th Chern number $N_{0{\rm Ch}}$ which is the number of eigenstates with negative eigenvalues of

$$\hat{H}_{0\Gamma} = i\left(\hat{H}_0 - E_{\rm ref}\mathbb{1}\right)\hat{\Gamma}. \tag{20}$$

Here, we have that $\hat{\Xi}$ and $\hat{\Gamma}$ are anti-commute with each other

$$\hat{\Xi}\hat{\Gamma} = -\hat{\Gamma}\hat{\Xi}. \tag{21}$$

In addition, we have supposed that the point-gap opens ($\det[\hat{H}_0 - E_{\rm ref}\mathbb{1}] \neq 0$) for $E_{\rm ref} \in i\mathbb{R}$. The above zero-th Chern number is previously introduced for the first-quantized Hamiltonian h[70,72,92].

The anti-commutation relation between $\hat{\Gamma}$ and $\hat{\Xi}$ is essential for the above topological characterization. For systems where $\hat{\Gamma}$ and $\hat{\Xi}$ commute with each other, $N_{0{\rm Ch}}$ does not characterize the topology due to the relation[113] $\hat{\Xi}\hat{H}_{0\Gamma} = -\hat{H}_{0\Gamma}\hat{\Xi}$.

In the above we have introduced the zero-dimensional $\mathbb{Z}$-invariant $N_{0{\rm Ch}}$ for chiral symmetric systems where $\hat{\Xi}$ satisfies Eq. (21).

2. Interacting case

In the presence of interactions, the second-quantized Hamiltonian is no longer quadratic, meaning that Eq. (18a) does not hold. However, we can still introduce the following $\mathbb{Z}_2$-invariant

$$\nu = {\rm sgn}\Big(\det[\hat{H} - E_{\rm ref}\mathbb{1}]\Big), \tag{22}$$

for $E_{\rm ref} \in \mathbb{R}$ due to the symmetry constraint (15). Here, ${\rm sgn}(x)$ takes 1 (-1) for $x > 0$ ($x < 0$).

In the non-interacting case, the parity of $N_{0{\rm Ch}}$ corresponds to ν for $E_{\rm ref} = 0$;

$$\nu = {\rm sgn}(\det[i\hat{\Gamma}])(-1)^{N_{0{\rm Ch}}}. \tag{23}$$

The above relation can be seen as follows

$$\begin{aligned}(-1)^{N_{0{\rm Ch}}} &= {\rm sgn}\Big(\det[\hat{H}_{0\Gamma}]\Big) \\ &= \nu\,{\rm sgn}\Big(\det[i\hat{\Gamma}]\Big),\end{aligned} \tag{24}$$

where we have used the relation $\det[i\hat{H}_0\hat{\Gamma}] = \det[i\hat{\Gamma}]\det[\hat{H}_0]$.

Equation (23) indicates that for the Fock space with N, the point-gap topological states form the $\mathbb{Z}$ group in the non-interacting case while the point-gap topological states form its subgroup $\mathbb{Z}_2$ in interacting cases. In particular, it indicates that interactions may destroy SPERs without breaking chiral symmetry if they are characterized by $\nu = 0$ and finite $N_{0{\rm Ch}}$.

B. Analysis of a toy model

The SPERs can be fragile against interactions due to the reduction of the non-Hermitian topological classification for systems with chiral symmetry. In order to demonstrate this fact, let us analyze a system described by the Hamiltonian with

$$\hat{H}_0 = \hat{\Psi}^\dagger h \hat{\Psi} + \sum_{\sigma=1,0,-1} i\gamma_\sigma\left(\hat{n}_{a\sigma} - \frac{1}{2}\right), \tag{25}$$

$$\hat{H}_{\rm int} = U \sum_{l=a,b} \left(\hat{n}_{l1} - \frac{1}{2}\right)\left(\hat{n}_{l-1} - \frac{1}{2}\right), \tag{26}$$

$$h = \left(\begin{array}{cc|cc|cc} 2i\beta & z^* & & & & \\ z & -2i\beta & & & & \\ \hline & & \frac{3}{2}i\beta & 2z^* & & \\ & & 2z & -\frac{3}{2}i\beta & & \\ \hline & & & & i\beta & 3z^* \\ & & & & 3z & -i\beta \end{array}\right). \tag{27}$$

Here, operators $\hat{\Psi}$ and $\hat{n}_{l\sigma}$ are defined as $\hat{\Psi} = (\hat{c}_{a1}, \hat{c}_{b1}|\hat{c}_{a0}, \hat{c}_{b0}|\hat{c}_{a-1}, \hat{c}_{b-1})^T$ and $\hat{n}_{l\sigma} = \hat{c}^\dagger_{l\sigma}\hat{c}_{l\sigma}$, respectively. Subscripts $l = a, b$ and $\sigma = 1, 0, -1$ label orbital and spin degrees of freedom[114], respectively. Parameters β, U and γ_σ are real numbers. A parameter z takes a complex number, $z = x + iy$ with $x, y \in \mathbb{R}$.

The Hamiltonian is chiral symmetric; $\hat{H}$ satisfies Eq. (15) with[70,115,116]

$$\hat{\Xi} = \prod_{\sigma=1,0,-1} (\hat{c}^\dagger_{a\sigma} + \hat{c}_{a\sigma})(\hat{c}^\dagger_{b\sigma} - \hat{c}_{b\sigma})\mathcal{K}. \tag{28}$$

Here, $\mathcal{K}$ is the complex-conjugation operator.

As well as chiral symmetry, the above Hamiltonian preserves charge U(1) symmetry and spin U(1) symmetry[117]; the Hamiltonian $\hat{H}$ satisfies

$$[\hat{H}, \hat{N}]_{\rm c} = 0, \tag{29}$$

$$[\hat{H}, \hat{S}_z]_{\rm c} = 0, \tag{30}$$

with $\hat{N} = \sum_{l\sigma} \hat{n}_{l\sigma}$ and $\hat{S}_z = \sum_{l\sigma} \sigma \hat{n}_{l\sigma}$. Thus, the Hamiltonian can be brock-diagonalized with respect to $\hat{N}$ and $\hat{S}_z$. By $\hat{H}_{(N,S_z)}$, we denote the second-quantized Hamiltonian for the Fock space with (N, S_z). Here, N and S_z denote eigenvalues of $\hat{N}$ and $\hat{S}_z$, respectively.

We demonstrate that $\hat{H}_{(3,0)}$ hosts an SPER characterized by the zero-th Chern number for $E_{\rm ref} = 0$ in the non-interacting case which is fragile against the interaction U. The emergence of the SPER at zero energy $E = 0$ can be observed in Figs. 3(a) and 3(b) (see red lines). On the SPER, four eigenvalues touch for both real- and imaginary-parts [see Figs. 3(c) and 3(d)]. In addition, Figs. 3(e) and 3(f) indicate that the zero-th Chern number for $E_{\rm ref} = 0$ jumps from $N_{\rm 0Ch} = 6$ to $N_{\rm 0Ch} = 4$ on the SPER with increasing x. The above results indicate that the system exhibits the SPER at zero energy $E = 0$ which is characterized by the zero-th Chern number, a $\mathbb{Z}$-invariant.

Here, the $\mathbb{Z}_2$-invariant ν does not change its value on the SPER; form Eq. (23) and Fig. 3(e), we can see that the $\mathbb{Z}_2$-invariant remains $\nu = 1$ for $E_{\rm ref} = 0$ by noting the relation $\det[i\hat{\Gamma}_{(3,0)}] = 1$.

The fact that the $\mathbb{Z}_2$-invariant does not jump on the SPER indicates the fragility of the SPER against the interaction U, which is demonstrated below. Figures 4(a) and 4(b) display the real- and imaginary-parts

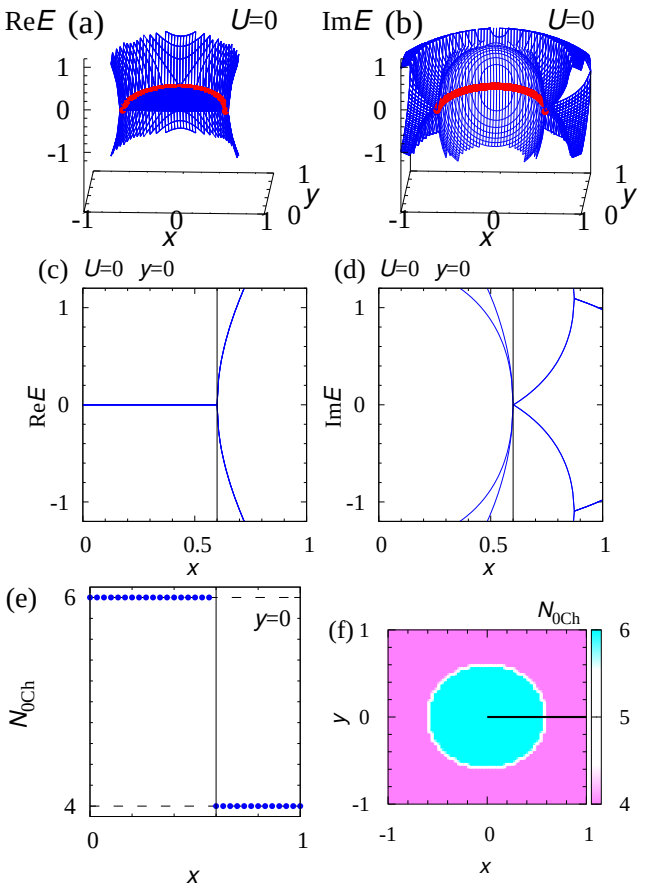

FIG. 3. Eigenvalues of $\hat{H}_{(3,0)}$ and its point-gap topology for $U = 0$. By $\hat{H}_{(3,0)}$, we denote the second-quantized Hamiltonian $\hat{H}$ for the Fock space with $(N, S_z) = (3, 0)$. (a) [(b)] The real- [imaginary-] part of the eigenvalues against x and y. The red lines denote the SPER. (c) [(d)] The real- [imaginary-] part of the eigenvalues for $y = 0$. (e) The zero-th Chern number $N_{\rm 0Ch}$ for $y = 0$. (f) Color plot of $N_{\rm 0Ch}$. The vertical lines in panels (c), (d), and (e) denote the critical value $x_c \sim 0.6$ where the band touching occurs. Data in panel (e) correspond to the zero-th Chern number on the black line in panel (f). These data are obtained for $(\beta, \gamma_1, \gamma_0, \gamma_{-1}) = (0.8, -3, -2.945, 1)$.

of the eigenvalues against x and y for $U = 0.2$. In contrast to the non-interacting case, the SPER cannot be observed; the real- and imaginary-parts do not touch simultaneously. The absence of the SPER can also be confirmed in Figs. 4(c) and 4(d). These numerical results demonstrate that the interaction U destroys the SPERs on which the zero-th Chern number jumps by an even number.

Putting the above results [Figs. 3 and 4 and Eq. (23)] together, we end up with the conclusion that the reduction $\mathbb{Z} \to \mathbb{Z}_2$ results in the fragility of the SPERs against interactions.

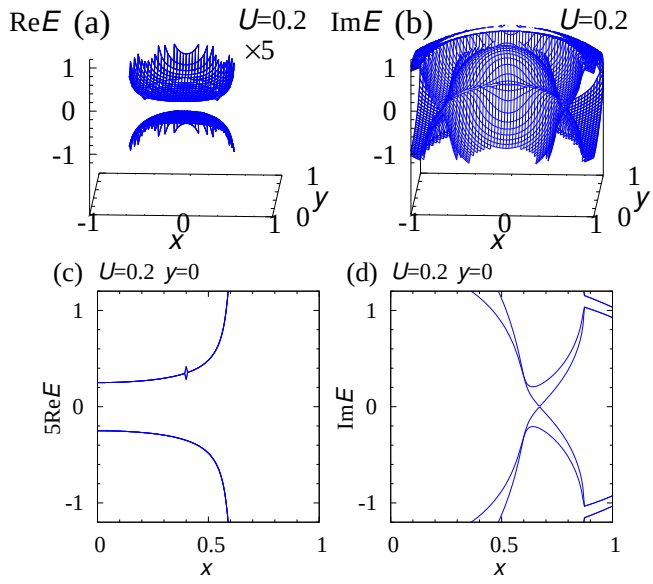

FIG. 4. Eigenvalues of $\hat{H}_{(3,0)}$ for $U = 0.2$. (a) [(b)] The real- [imaginary-] parts of the eigenvalues against x and y. (c) [(d)] The real- [imaginary-] parts of the eigenvalues for $y = 0$. Panel (c) displays the data multiplied by 5 [i.e., $5\mathrm{Re}E_n$ $n = 1, 2, \ldots, 8$]. These data are obtained for $(\beta, \gamma_1, \gamma_0, \gamma_{-1}) = (0.8, -3, -2.945, 1)$.

IV. SUMMARY

We have addressed interaction effects on the EPs and the SPERs in the two-dimensional parameter space. Our analysis elucidates that interactions may destroy the EPs and the SPERs without breaking relevant symmetry. The fragility of EPs and the SPERs is due to the reduction of the non-Hermitian topological classification. Specifically, we have seen that the reduction $\mathbb{Z}^{(N+P'+1)/2} \to \mathbb{Z}$ ($\mathbb{Z} \to \mathbb{Z}_2$) results in the fragility of EPs (SPERs) for systems with charge U(1) symmetry and spin-parity symmetry (chiral symmetry). The above results strongly suggest that the reduction of topological classifications results in the fragility of EPs and their variants in generic dimensions and symmetry classes.

We finish this paper with a remark on gapped systems. Topological invariants defined in Eqs. (5) and (6) [Eqs. (20) and (22)] are available for the characterization of one- [zero-] dimensional gapped systems. In particular, Eqs. (5), (6), and (7) indicate the reduction of one-dimensional point-gap topology $\mathbb{Z}^{(N+P'+1)/2} \to \mathbb{Z}$ for gapped systems with charge U(1) and spin-parity symmetry (see Appendix C). In addition, Eqs. (20), (22), and (23) indicate the reduction of zero-dimensional point-gap topology $\mathbb{Z} \to \mathbb{Z}_2$ for gapped systems with chiral symmetry (see Appendix D).

ACKNOWLEDGEMENTS

The authors thank Hosho Katsura, Norio Kawakami, and Takuma Isobe for fruitful discussions. A part of the computation has been done using the facilities of the Supercomputer Center, the Institute for Solid State Physics, the University of Tokyo. This work is supported by JSPS KAKENHI Grants No. 17H06138, No. JP21K13850 and No. JP22H05247. This work is also supported by JST CREST, Grant No. JPMJCR19T1.

[1] D. C. Tsui, H. L. Stormer, and A. C. Gossard, Phys. Rev. Lett. **48**, 1559 (1982).
[2] R. B. Laughlin, Phys. Rev. Lett. **50**, 1395 (1983).
[3] E. Tang, J.-W. Mei, and X.-G. Wen, Phys. Rev. Lett. **106**, 236802 (2011).
[4] K. Sun, Z. Gu, H. Katsura, and S. Das Sarma, Phys. Rev. Lett. **106**, 236803 (2011).
[5] T. Neupert, L. Santos, C. Chamon, and C. Mudry, Phys. Rev. Lett. **106**, 236804 (2011).
[6] N. Regnault and B. A. Bernevig, Phys. Rev. X **1**, 021014 (2011).
[7] D. N. Sheng, Z.-C. Gu, K. Sun, and L. Sheng, Nature Communications **2**, 389 EP (2011), article.
[8] E. J. Bergholtz and Z. Liu, International Journal of Modern Physics B **27**, 1330017 (2013).
[9] D. Pesin and L. Balents, Nature Physics **6**, 376 (2010).
[10] A. P. Schnyder, S. Ryu, A. Furusaki, and A. W. W. Ludwig, Phys. Rev. B **78**, 195125 (2008).
[11] A. Kitaev, AIP Conf. Proc. **1134**, 22 (2009).
[12] S. Ryu, A. P. Schnyder, A. Furusaki, and A. W. W. Ludwig, New J. Phys. **12**, 065010 (2010).
[13] L. Fidkowski and A. Kitaev, Phys. Rev. B **81**, 134509 (2010).
[14] F. Pollmann, A. M. Turner, E. Berg, and M. Oshikawa, Phys. Rev. B **81**, 064439 (2010).
[15] A. M. Turner, F. Pollmann, and E. Berg, Phys. Rev. B **83**, 075102 (2011).
[16] L. Fidkowski and A. Kitaev, Phys. Rev. B **83**, 075103 (2011).
[17] X. Chen, Z.-C. Gu, and X.-G. Wen, Phys. Rev. B **83**, 035107 (2011).
[18] X. Chen, Z.-C. Gu, and X.-G. Wen, Phys. Rev. B **84**, 235128 (2011).
[19] Y.-M. Lu and A. Vishwanath, Phys. Rev. B **86**, 125119 (2012).
[20] H. Yao and S. Ryu, Phys. Rev. B **88**, 064507 (2013).
[21] S. Ryu and S.-C. Zhang, Phys. Rev. B **85**, 245132 (2012).
[22] X.-L. Qi, New J. Phys. **15**, 065002 (2013).
[23] M. Levin and A. Stern, Phys. Rev. B **86**, 115131 (2012).
[24] C.-T. Hsieh, T. Morimoto, and S. Ryu, Phys. Rev. B **90**, 245111 (2014).
[25] H. Isobe and L. Fu, Phys. Rev. B **92**, 081304 (2015).
[26] X. Chen, Z.-C. Gu, Z.-X. Liu, and X.-G. Wen, Phys. Rev. B **87**, 155114 (2013).
[27] Z.-C. Gu and X.-G. Wen, Phys. Rev. B **90**, 115141 (2014).
[28] A. Kapustin, arXiv:1403.1467 (2014).
[29] A. Kapustin, arXiv:1404.6659 (2014).

[30] A. Kapustin, R. Thorngren, A. Turzillo, and Z. Wang, Journal of High Energy Physics **2015**, 1 (2015).
[31] L. Fidkowski, X. Chen, and A. Vishwanath, Phys. Rev. X **3**, 041016 (2013).
[32] C. Wang, A. C. Potter, and T. Senthil, **343**, 629 (2014).
[33] M. A. Metlitski, L. Fidkowski, X. Chen, and A. Vishwanath, arXiv:1406.3032 (2014).
[34] C. Wang and T. Senthil, Phys. Rev. B **89**, 195124 (2014).
[35] Y.-Z. You and C. Xu, Phys. Rev. B **90**, 245120 (2014).
[36] T. Morimoto, A. Furusaki, and C. Mudry, Phys. Rev. B **92**, 125104 (2015).
[37] T. Yoshida, A. Daido, Y. Yanase, and N. Kawakami, Phys. Rev. Lett. **118**, 147001 (2017).
[38] C.-M. Jian and C. Xu, Phys. Rev. X **8**, 041030 (2018).
[39] Y. C. Hu and T. L. Hughes, Phys. Rev. B **84**, 153101 (2011).
[40] K. Esaki, M. Sato, K. Hasebe, and M. Kohmoto, Phys. Rev. B **84**, 205128 (2011).
[41] M. Sato, K. Hasebe, K. Esaki, and M. Kohmoto, Progress of Theoretical Physics **127**, 937 (2012).
[42] S. Diehl, E. Rico, M. A. Baranov, and P. Zoller, Nature Physics **7**, 971 (2011).
[43] C.-E. Bardyn, M. A. Baranov, C. V. Kraus, E. Rico, A. İmamoğlu, P. Zoller, and S. Diehl, New Journal of Physics **15**, 085001 (2013).
[44] J. C. Budich, P. Zoller, and S. Diehl, Phys. Rev. A **91**, 042117 (2015).
[45] T. E. Lee, Phys. Rev. Lett. **116**, 133903 (2016).
[46] Z. Gong, S. Higashikawa, and M. Ueda, Phys. Rev. Lett. **118**, 200401 (2017).
[47] S. Lieu, Phys. Rev. B **97**, 045106 (2018).
[48] Z. Gong, Y. Ashida, K. Kawabata, K. Takasan, S. Higashikawa, and M. Ueda, Phys. Rev. X **8**, 031079 (2018).
[49] K. Kawabata, K. Shiozaki, M. Ueda, and M. Sato, Phys. Rev. X **9**, 041015 (2019).
[50] S. Lieu, M. McGinley, and N. R. Cooper, Phys. Rev. Lett. **124**, 040401 (2020).
[51] E. J. Bergholtz, J. C. Budich, and F. K. Kunst, Rev. Mod. Phys. **93**, 015005 (2021).
[52] Y. Ashida, Z. Gong, and M. Ueda, Advances in Physics **69**, 249 (2020).
[53] V. M. Martinez Alvarez, J. E. Barrios Vargas, and L. E. F. Foa Torres, Phys. Rev. B **97**, 121401 (2018).
[54] S. Yao and Z. Wang, Phys. Rev. Lett. **121**, 086803 (2018).
[55] F. K. Kunst, E. Edvardsson, J. C. Budich, and E. J. Bergholtz, Phys. Rev. Lett. **121**, 026808 (2018).
[56] C. H. Lee and R. Thomale, Phys. Rev. B **99**, 201103 (2019).
[57] D. S. Borgnia, A. J. Kruchkov, and R.-J. Slager, Phys. Rev. Lett. **124**, 056802 (2020).
[58] K. Zhang, Z. Yang, and C. Fang, Phys. Rev. Lett. **125**, 126402 (2020).
[59] N. Okuma, K. Kawabata, K. Shiozaki, and M. Sato, Phys. Rev. Lett. **124**, 086801 (2020).
[60] T. Hofmann, T. Helbig, F. Schindler, N. Salgo, M. Brzezińska, M. Greiter, T. Kiessling, D. Wolf, A. Vollhardt, A. Kabaši, C. H. Lee, A. Bilušić, R. Thomale, and T. Neupert, Phys. Rev. Research **2**, 023265 (2020).
[61] T. Yoshida, T. Mizoguchi, and Y. Hatsugai, Phys. Rev. Research **2**, 022062 (2020).
[62] H. Shen, B. Zhen, and L. Fu, Phys. Rev. Lett. **120**, 146402 (2018).
[63] Y. Xu, S.-T. Wang, and L.-M. Duan, Phys. Rev. Lett. **118**, 045701 (2017).
[64] A. U. Hassan, B. Zhen, M. Soljačić, M. Khajavikhan, and D. N. Christodoulides, Phys. Rev. Lett. **118**, 093002 (2017).
[65] H. Zhou, C. Peng, Y. Yoon, C. W. Hsu, K. A. Nelson, L. Fu, J. D. Joannopoulos, M. Soljačić, and B. Zhen, Science **359**, 1009 (2018).
[66] V. Kozii and L. Fu, arXiv preprint arXiv:1708.05841 (2017).
[67] T. Yoshida, R. Peters, and N. Kawakami, Phys. Rev. B **98**, 035141 (2018).
[68] J. C. Budich, J. Carlström, F. K. Kunst, and E. J. Bergholtz, Phys. Rev. B **99**, 041406 (2019).
[69] R. Okugawa and T. Yokoyama, Phys. Rev. B **99**, 041202 (2019).
[70] T. Yoshida, R. Peters, N. Kawakami, and Y. Hatsugai, Phys. Rev. B **99**, 121101 (2019).
[71] H. Zhou, J. Y. Lee, S. Liu, and B. Zhen, Optica **6**, 190 (2019).
[72] K. Kawabata, T. Bessho, and M. Sato, Phys. Rev. Lett. **123**, 066405 (2019).
[73] P. Delplace, T. Yoshida, and Y. Hatsugai, Phys. Rev. Lett. **127**, 186602 (2021).
[74] I. Mandal and E. J. Bergholtz, Phys. Rev. Lett. **127**, 186601 (2021).
[75] P. San-Jose, J. Cayao, E. Prada, and R. Aguado, Scientific Reports **6**, 21427 (2016).
[76] T. Ozawa, H. M. Price, A. Amo, N. Goldman, M. Hafezi, L. Lu, M. C. Rechtsman, D. Schuster, J. Simon, O. Zilberberg, and I. Carusotto, Rev. Mod. Phys. **91**, 015006 (2019).
[77] T. Yoshida and Y. Hatsugai, Phys. Rev. B **100**, 054109 (2019).
[78] Y. Li, Y.-G. Peng, L. Han, M.-A. Miri, W. Li, M. Xiao, X.-F. Zhu, J. Zhao, A. Alù, S. Fan, and C.-W. Qiu, **364**, 170 (2019).
[79] M. Partanen, J. Goetz, K. Y. Tan, K. Kohvakka, V. Sevriuk, R. E. Lake, R. Kokkoniemi, J. Ikonen, D. Hazra, A. Mäkinen, E. Hyyppä, L. Grönberg, V. Vesterinen, M. Silveri, and M. Möttönen, Phys. Rev. B **100**, 134505 (2019).
[80] M. Naghiloo, M. Abbasi, Y. N. Joglekar, and K. W. Murch, Nature Physics **15**, 1232 (2019).
[81] T. Yoshida, T. Mizoguchi, and Y. Hatsugai, Scientific Reports **12**, 560 (2022).
[82] D. J. Luitz and F. Piazza, Phys. Rev. Research **1**, 033051 (2019).
[83] T. Yoshida, K. Kudo, and Y. Hatsugai, Scientific Reports **9**, 16895 (2019).
[84] T. Yoshida, K. Kudo, H. Katsura, and Y. Hatsugai, Phys. Rev. Research **2**, 033428 (2020).
[85] C.-X. Guo, X.-R. Wang, C. Wang, and S.-P. Kou, Phys. Rev. B **101**, 144439 (2020).
[86] N. Matsumoto, K. Kawabata, Y. Ashida, S. Furukawa, and M. Ueda, Phys. Rev. Lett. **125**, 260601 (2020).
[87] D.-W. Zhang, Y.-L. Chen, G.-Q. Zhang, L.-J. Lang, Z. Li, and S.-L. Zhu, Phys. Rev. B **101**, 235150 (2020).
[88] T. Liu, J. J. He, T. Yoshida, Z.-L. Xiang, and F. Nori, Phys. Rev. B **102**, 235151 (2020).
[89] Z. Xu and S. Chen, Phys. Rev. B **102**, 035153 (2020).
[90] L. Pan, X. Wang, X. Cui, and S. Chen, Phys. Rev. A **102**, 023306 (2020).
[91] S. Mu, C. H. Lee, L. Li, and J. Gong, Phys. Rev. B **102**, 081115 (2020).

[92] T. Yoshida and Y. Hatsugai, Phys. Rev. B **104**, 075106 (2021).
[93] K. Yang, S. C. Morampudi, and E. J. Bergholtz, Phys. Rev. Lett. **126**, 077201 (2021).
[94] R. Shen and C. H. Lee, Communications Physics **5**, 238 (2022).
[95] C. H. Lee, Phys. Rev. B **104**, 195102 (2021).
[96] S.-B. Zhang, M. M. Denner, T. c. v. Bzdušek, M. A. Sentef, and T. Neupert, Phys. Rev. B **106**, L121102 (2022).
[97] K. Kawabata, K. Shiozaki, and S. Ryu, Phys. Rev. B **105**, 165137 (2022).
[98] R. Schäfer, J. C. Budich, and D. J. Luitz, arXiv preprint arXiv:2204.05340 (2022).
[99] T. Orito and K.-I. Imura, Phys. Rev. B **105**, 024303 (2022).
[100] S. Tsubota, H. Yang, Y. Akagi, and H. Katsura, Phys. Rev. B **105**, L201113 (2022).
[101] W. N. Faugno and T. Ozawa, arXiv preprint arXiv:2210.01572 (2022).
[102] T. Yoshida and Y. Hatsugai, arXiv preprint arXiv:2205.09333 (2022).
[103] F. Qin, R. Shen, and C. H. Lee, arXiv preprint arXiv:2202.10481 (2022).
[104] T. Tomita, S. Nakajima, I. Danshita, Y. Takasu, and Y. Takahashi, Science Advances **3**, e1701513 (2017).
[105] T. Tomita, S. Nakajima, Y. Takasu, and Y. Takahashi, Phys. Rev. A **99**, 031601 (2019).
[106] Y. Takasu, T. Yagami, Y. Ashida, R. Hamazaki, Y. Kuno, and Y. Takahashi, Progress of Theoretical and Experimental Physics **2020**, 12A110 (2020).
[107] R. Ma, B. Saxberg, C. Owens, N. Leung, Y. Lu, J. Simon, and D. I. Schuster, Nature **566**, 51 (2019).
[108] We have imposed the additional constraint on the $\hat{H}$. However, this does not affect the discussion provided in Sec. II A because the argument in Sec. II A is directly available by replacing the $\hat{H}$ to the block-diagonalized Hamiltonian with $\sum_\sigma \hat{n}_\sigma$.
[109] Specifically, the winding numbers take $W_{(2,0)} = W_{[2,-1]} = 0$ for $V = 0$.
[110] This 4×4-matrix is diagonalized as follows. The Hamiltonian can be rewritten as

$$\hat{H}_{(2,1)} = \begin{pmatrix} e^{i\frac{\theta}{2}} M_\theta & iV\tau_0 \\ iV\tau_0 & e^{-i\frac{\theta}{2}} M_\theta \end{pmatrix}. \tag{31}$$

Here, the 2×2 identity matrix is denoted by τ_0. The matrix M_θ is defined as $M_\theta = \begin{pmatrix} 0 & e^{i\frac{\theta}{2}} \\ e^{-i\frac{\theta}{2}} & 0 \end{pmatrix}$. Thus, firstly diagonazling the matrix M_θ, we obtain the eigenvalues shown in Eq. (14) .
[111] We note that $\xi^2 = \mathbb{1}$ holds due to the relations $u_{\rm T} u_{\rm T}^* = \pm\mathbb{1}$ and $u_{\rm C} u_{\rm C}^* = \pm\mathbb{1}$. Here $u_{\rm T}$ ($u_{\rm C}$) denotes a unitary matrix describing time-reversal (particle-hole) symmetry.
In order to obtain the relation $\xi^2 = \mathbb{1}$, we note that $u_{\rm T} u_{\rm C}^*$ squares to be $\pm\mathbb{1}$; $(u_{\rm T} u_{\rm C}^*)(u_{\rm T} u_{\rm C}^*) = u_{\rm T} u_{\rm T}^* u_{\rm C} u_{\rm C}^*$. Here we have used the fact that without loss of generality, $u_{\rm T}$ and $u_{\rm C}$ can be chosen so that $u_{\rm T} u_{\rm C}^* = u_{\rm C} u_{\rm T}^*$ is satisfied.
For $(u_{\rm T} u_{\rm C}^*)^2 = \mathbb{1}$, we can define ξ as $\xi = u_{\rm T} u_{\rm C}^*$. For $(u_{\rm T} u_{\rm C}^*)^2 = -\mathbb{1}$, we can define ξ as $\xi = i u_{\rm T} u_{\rm C}^*$. Therefore, we can see that $\xi^2 = \mathbb{1}$ holds .
[112] This fact can be directly seen by noting that $h_{\rm H}$ is written as $h_{\rm H} = \left(\begin{array}{c|c} 0 & q \\ \hline q^\dagger & 0 \end{array}\right)$ with the basis where ξ is written as $\xi = \left(\begin{array}{c|c} \mathbb{1} & 0 \\ \hline 0 & -\mathbb{1} \end{array}\right)$. Here, q is a matrix. We also note that $h_{\rm A}$ is written as $h_{\rm A} = \left(\begin{array}{c|c} q_{\rm A+} & 0 \\ \hline 0 & q_{\rm A-} \end{array}\right)$ with the above basis. Here, q_{A+} and q_{A-} are anti-Hermitian matrices.
[113] For systems where $\hat{\Gamma}$ and $\hat{\Xi}$ commute each other, consider an eigenstate $|\tilde{E}\rangle$ of the Hermitian operator $\hat{H}_{0\Gamma}$ with eigenvalue $\tilde{E} \in \mathbb{R}$. Then, we have $\hat{H}_{0\Gamma}\hat{\Xi}|\tilde{E}\rangle = -\tilde{E}\hat{\Xi}|\tilde{E}\rangle$, meaning that the state $\hat{\Xi}|\tilde{E}\rangle$ is an eigenstate with eigenvalue $-\tilde{E}$. Thus, tuning parameters does not change the zero-th Chern number $N_{0\rm Ch}$ when $\hat{\Gamma}$ and $\hat{\Xi}$ commute each other. In contrast, for systems where $\hat{\Gamma}$ and $\hat{\Xi}$ anticommute each other [see Eq. (21)], the zero-th Chern number $N_{0\rm Ch}$ can change its value; in this case, the relation $\hat{\Xi}\hat{H}_{0\Gamma} = \hat{H}_{0\Gamma}\hat{\Xi}$ holds .
[114] To be strict, the subscript $\sigma = 1, 0, -1$ labels pseudospin because fermions should have odd half-integer spin $(1/2, 3/2, 5/2 \ldots)$.
[115] V. Gurarie, Phys. Rev. B **83**, 085426 (2011).
[116] S. R. Manmana, A. M. Essin, R. M. Noack, and V. Gurarie, Phys. Rev. B **86**, 205119 (2012).
[117] We have imposed the additional constraints on the $\hat{H}$. However, these constraints do not affect the discussion provided in Sec. III A because the block-diagonalization is not effected by the presence/absence of interactions in contrast to the case of Sec. II A. Namely, the argument in Sec. III A is directly available by replacing the $\hat{H}$ to the block-diagonalized Hamiltonian with $\hat{N}$ and $\hat{S}_z$, although an explicit analysis of a toy model without additional symmetry constraints is left as a future work .

Appendix A: The number of the subspaces for the Fock space with $[N, P]$

For a given set of $[N, P]$, we count how many sets of $(N_\uparrow, N_\downarrow)$ are allowed, which elucidates the number of the subspaces for the given Fock space with $[N, P]$. We count the number of the sets $(N_\uparrow, N_\downarrow)$ for the following four cases.

(i) For even N and $P = 1$, the following sets of $(N_\uparrow, N_\downarrow)$ are allowed:

$$\{(2M, 0), (2M-2, 2), (2M-4, 4), \ldots, (0, 2M)\}, \tag{A1}$$

with $N = 2M$ and M being a non-negative integer. Thus, there exist the number $N/2 + 1$ of the sets $(N_\uparrow, N_\downarrow)$ for the given set of $[N, P] = [2M, 1]$.

(ii) For even N and $P = -1$, the following sets of $(N_\uparrow, N_\downarrow)$ are allowed:

$$\{(2M-1, 1), (2M-3, 3), (2M-5, 5), \ldots, (1, 2M-1)\}, \tag{A2}$$

with $N = 2M$ and M being a non-negative integer. Thus, there exist the number $N/2$ of the sets $(N_\uparrow, N_\downarrow)$ for the given set of $[N, P] = [2M, -1]$.

(iii) For odd N and $P = 1$, the following sets of

$(N_\uparrow, N_\downarrow)$ are allowed:

$$\{(2M+1,0),(2M-1,2),(2M-3,4),\ldots,(1,2M)\}\,, \tag{A3}$$

with $N = 2M+1$ and M being a non-negative integer. Thus, there exist the number $(N+1)/2$ of the sets $(N_\uparrow, N_\downarrow)$ for the given set of $[N,P] = [2M+1, 1]$.

(iv) For odd N and $P = -1$, the following sets of $(N_\uparrow, N_\downarrow)$ are allowed:

$$\{(2M,1),(2M-2,3),(2M-4,5),\ldots,(0,2M+1)\}\,, \tag{A4}$$

with $N = 2M+1$ and M being a non-negative integer. Thus, there exist the number $(N+1)/2$ of the sets $(N_\uparrow, N_\downarrow)$ for the given set of $[N,P] = [2M+1, -1]$.

Taking into account the above results, we end up with the fact that there exist the number $(N+P'+1)/2$ of the subspaces with $(N_\uparrow, N_\downarrow)$ for the given Fock space with $[N,P]$. Here, P' takes P (0) for even (odd) N.

Appendix B: Robustness of EPs for $s_\downarrow = 1$

EPs characterized by a finite value of the winding number $W_{[N,P]}$ are robust against interactions. In order to demonstrate this fact, let us analyze the Hamiltonian discussed in Sec. II B for $s_\downarrow = 1$ [i.e., the Hamiltonian (1) specified by Eqs. (8) and (9)].

As is the case of $s_\downarrow = -1$ (see Sec. II B), we focus on the Fock space with $[N,P] = [2,1]$. Figures 5(a) and 5(b)

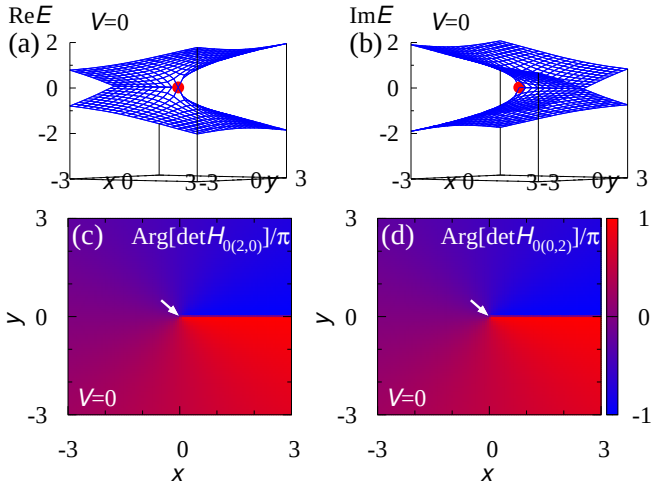

FIG. 5. (a) [(b)] The real- [imaginary-] part of eigenvalues of $\hat{H}_{[2,1]}$ for $V = 0$ and $s_\downarrow = 1$. The red dots denote EPs. (c) [(d)] The argument of $\det\hat{H}_{0(2,0)}$ [$\det\hat{H}_{0(0,2)}$]. The data are plotted in a similar way to Fig. 1.

display eigenvalues of $\hat{H}_{[2,1]}$ for $V = 0$ and $s_\downarrow = 1$. For $V = 0$, the Fock space can be divided into subspaces with $(N_\uparrow, N_\downarrow) = (2,0)$ and $(0,2)$. For both subspaces, EPs emerge which are characterized by the winding numbers $(W_{(2,0)}, W_{(0,2)}) = (1,1)$ for $E_{\rm ref} = 0$ [see Figs. 5(c) and 5(d)]. Thus, recalling Eq. (7), we have $W_{[N,P]} = 2$ for $E_{\rm ref} = 0$. This result is consistent with Fig. 6(a); $W_{[N,P]}$ takes two which is computed along a path winding around the singular point (denoted by a white arrow) in the counterclockwise direction.

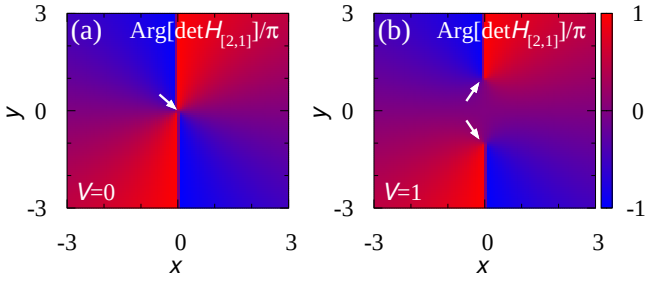

FIG. 6. (a) [(b)] The argument of $\det\hat{H}_{[2,1]}$ for $V = 0$ [$V = 1$] and $s_\downarrow = 1$. The white arrows indicate the points where EPs emerge.

The finite value of $W_{[N,P]}$ in the non-interacting case indicates the robustness of EPs against interactions. Figure 6(b) displays color map of $\det\hat{H}_{[2,1]}$ for $V = 1$. In this figure, we can see that $W_{[N,P]}$ takes one which is computed along a path winding around the singular point (denoted by a white arrow) in the counterclockwise direction. Correspondingly, the EPs emerges even in the

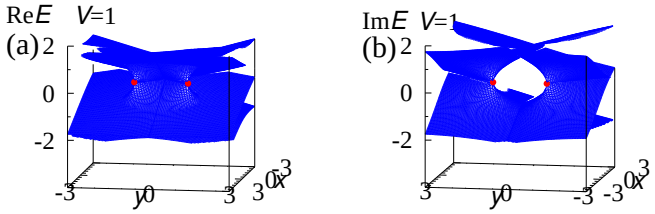

FIG. 7. (a) [(b)] The real- [imaginary-] part of eigenvalues of $\hat{H}_{[2,1]}$ for $V = 1$ and $s_\downarrow = 1$. Red dots denote the EPs at zero energy $E = 0$. The data are plotted in a similar way to Fig. 2.

interacting cases. Figure 7 displays eigenvalues of $\hat{H}_{[2,1]}$ for $V = 1$ and $s_\downarrow = 1$. The above results indicate that EPs characterized by a finite value of $W_{[N,P]}$ are robust against interactions.

Appendix C: Reduction of one-dimensional topology for gapped systems

Computing the topological invariants [Eqs. (5) and (6)], we analyze the one-dimensional topology of a gapped system, which justifies the reduction $\mathbb{Z}^{(N+P'+1)/2} \to \mathbb{Z}$ for the one-dimensional point-gap topology with charge U(1) symmetry and spin-parity symmetry. In the following, the topology in a one-dimensional parameter space is mainly analyzed, although a similar analysis can be done for the topology

in one spatial dimension as briefly explained around the end of this section.

Consider the Hamiltonian (1) specified with $\hat{\Psi} = (\hat{c}_{a\uparrow}, \hat{c}_{b\uparrow}, \hat{c}_{a\downarrow}, \hat{c}_{b\downarrow})^T$,

$$h(\theta) = \mathrm{diag}(e^{i\theta}, 0, e^{-i\theta}, 0), \tag{C1}$$

$$\hat{H}_{\mathrm{int}} = iV[\hat{S}_a^+ \hat{S}_b^+ + \hat{S}_a^- \hat{S}_b^-]. \tag{C2}$$

Here, diag(...) denotes a diagonal matrix whose elements are specified by the numbers enclosed in the parentheses. The coefficient V is a real number. The one-dimensional parameter space is described by θ ($0 \le \theta < 2\pi$).

The above Hamiltonian preserves charge U(1) symmetry and spin-parity symmetry [see Eqs. (2a) and (2b)]. We also note that $\hat{H}$ commutes with $\hat{n}_{b\sigma} = \hat{c}^\dagger_{b\sigma}\hat{c}_{b\sigma}$ for $\sigma = \uparrow, \downarrow$. Thus, we suppose that a fermion occupies orbital b.

For the Fock space with $[N, P] = [2, 1]$, the Hamiltonian is written as

$$\hat{H}_{[2,1]} = \begin{pmatrix} e^{i\theta} & iV \\ iV & e^{-i\theta} \end{pmatrix}, \tag{C3}$$

with the basis

$$\left(\hat{c}^\dagger_{a\uparrow}\hat{c}^\dagger_{b\uparrow}|0\rangle,\ \hat{c}^\dagger_{a\downarrow}\hat{c}^\dagger_{b\downarrow}|0\rangle\right). \tag{C4}$$

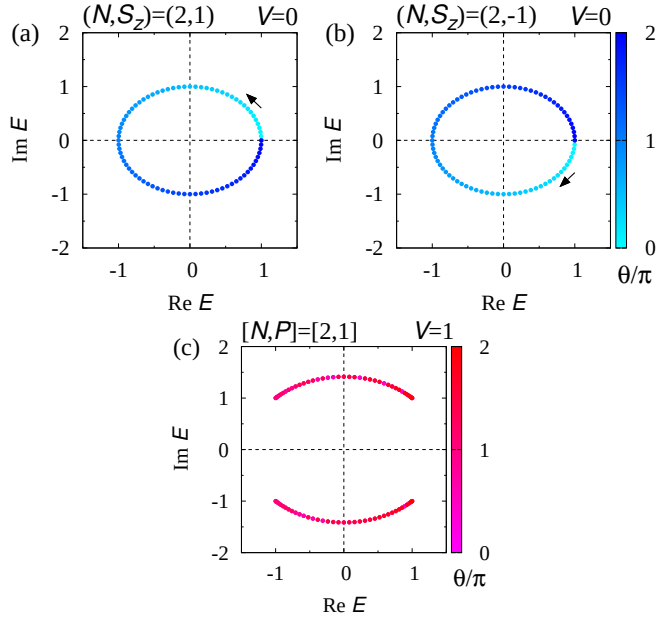

FIG. 8. Spectral flow of the Hamiltonian $\hat{H}$ for the Fock space with $[N, P] = [2, 1]$. (a) [(b)] Spectral flow for the subspaces with $(N, S_z) = (2, 1)$ [$(2, -1)$] at $V = 0$. (c) Spectral flow for the Fock space with $[N, P] = [2, 1]$ at $V = 1$.

For $V = 0$, the above representation indicates that the Fock space is decomposed into subspaces with $(N, S_z) = (2, 1)$ and $(2, -1)$, and that the winding numbers for these subspaces take $W_{(2,1)} = 1$ and $W_{(2,-1)} = -1$ at $E_{\mathrm{ref}} = 0$, respectively [see Figs. 8(a) and 8(b)]. Therefore, the loop structures observed in Figs. 8(a) and 8(b) are robust against perturbations at the non-interacting level because they are protected by the non-trivial point-gap topology.

Here, Eq. (7) indicates that the above loop structure is no longer protected by the non-trivial topology in the presence of interactions; because of the winding numbers $W_{(2,1)} = 1$ and $W_{(2,1)} = -1$ for $E_{\mathrm{ref}} = 0$, Eq. (7) results in $W_{[2,1]} = 0$. Indeed, the interaction V destroys the loop structure observed in Figs. 8(a) and 8(b). In order to see this, we compute the eigenvalues which are written as

$$E_\pm(\theta) = \cos\theta \pm i\sqrt{\sin^2\theta + V^2}. \tag{C5}$$

This result elucidates that the loop structure is destroyed by interactions mixing the subspaces with $(N, S_z) = (2, 1)$ and $(2, -1)$; $|\mathrm{Im}E_\pm(\theta)| > 0$ holds for an arbitrary θ. This fact is explicitly presented in Fig. 8(c).

The above results demonstrate that the reduction of the one-dimensional point-gap topology for the gapped systems: $\mathbb{Z}^2 \to \mathbb{Z}$ for $[N, P] = [2, 1]$. Namely, in the non-interacting case, the second quantized Hamiltonian $\hat{H}_0$ possesses the non-trivial properties characterized by $W_{(2,1)} = 1$ and $W_{(2,-1)} = -1$ for $E_{\mathrm{ref}} = 0$. However, the non-trivial topology is not maintained in the presence of interactions ($W_{[2,1]} = 0$), which is supported by the fragility of the loop structure against the interactions [see Fig. 8].

We finish this section with two remarks. The previous work[102] has also addressed the reduction phenomena. We note, however, that Ref. 102 has compared the topology of the first-quantized Hamiltonian h and the second-quantized Hamiltonian $\hat{H}$. In contrast, the analysis provided in this section compares the topology of the non-interacting second-quantized Hamiltonian $\hat{H}_0$ with that of the interacting second-quantized Hamiltonian $\hat{H}$ which clearly elucidates that the $\mathbb{Z}^{(N+P'+1)/2}$ group formed by the point-gap topological states in non-interacting cases reduces to its subgroup $\mathbb{Z}$ due to the interactions [see Eq. (7)].

We also note that a similar argument is applied to the point-gap topology in one spatial dimension. In Ref. 102, the point-gap topology in one spatial dimension is analyzed for an interacting non-Hermitian chain with charge U(1) symmetry and spin-parity symmetry [see Eq. (9) of Ref. 102]. Because the Fock space with $[N, P] = [3, -1]$ is divided into subspaces with $(N, S_z) = (3, 3/2)$ and $(3, -1/2)$ in the non-interacting case, the topology of non-interacting Hamiltonian is characterized by the two winding numbers taking $W_{(3,3/2)} = 1$ and $W_{(3,-1/2)} = -1$ at $E_{\mathrm{ref}} = 0$ for the Fock space with $[N, P] = [3, -1]$. Thus, the loop structure is observed for the non-interacting non-Hermitian chain [see Fig. 3(b) of Ref. 102]. This loop structure is fragile against interactions because Eq. (7) results in the vanishing winding number $W_{[N,P]} = 0$. Indeed, interactions destroy the loop structure with keeping the point-gap for $E_{\mathrm{ref}} = 0$ and the relevant symmetry [see Fig. 3(d) of Ref. 102]. Correspondingly, the non-Hermitian skin effect observed

at the non-interacting level is also destroyed by the interactions [see Figs. 3(c) and 3(e) of Ref. 102].

Appendix D: Reduction of zero-dimensional topology for a gapped system

We analyze the zero-dimensional topology of a gapped system, which justifies the reduction $\mathbb{Z} \to \mathbb{Z}_2$ for the zero-dimensional point-gap topology with chiral symmetry. Although the following results are essentially the same as the ones in Sec. III B, we discuss the details by focusing on a zero-dimensional system with the point-gap.

Consider the Hamiltonian $\hat{H}$ specified with Eqs. (25), (26), and (27) for given real parameters x and $y = 0$ (i.e., $z = x$, $0 \le x \le 1$). The Hamiltonian $\hat{H}$ preserves the chiral symmetry (15) with $\hat{\Xi}$ defined in Eq. (28). Thus, in the absence of interactions, the topology of $\hat{H}$ is characterized by the zero-th Chern number $N_{0\mathrm{Ch}}$, a $\mathbb{Z}$-invariant [see Sec. III A 1]. In the presence of interactions, the topology of $\hat{H}$ is characterized by the $\mathbb{Z}_2$-invariant ν.

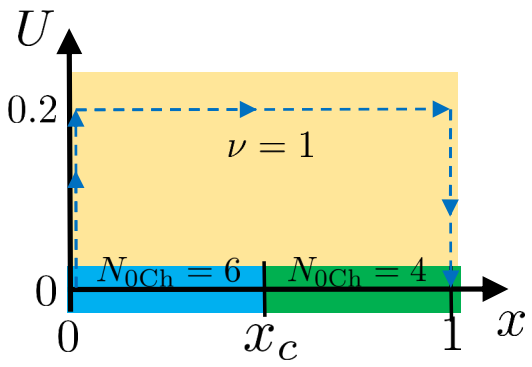

FIG. 9. Phase diagram of the Hamiltonian $\hat{H}_{(3,0)}$. In the absence of interactions, the zero-th Chern number takes $N_{0\mathrm{Ch}} = 4$ (6) at $E_{\mathrm{ref}} = 0$ for $0 \le x < x_c$ ($x_c < x \le 1$) with $x_c \sim 0.6$. In the presence of interaction, the $\mathbb{Z}_2$-invariant takes $\nu = 1$ for $0 \le x \le 1$. Dashed allows illustrate a path parameterized by λ.

Let us focus on the Fock space with $(N, S_z) = (3, 0)$. Figure 9 displays topological invariants against x and U. In the non-interacting case, the point-gap at $E_{\mathrm{ref}} = 0$ closes ($\det \hat{H}_{(3,0)} = 0$) at the point $(x, U) = (x_c, 0)$ with $x_c \sim 0.6$ which separates two regions of distinct point-gap topology with $N_{0\mathrm{Ch}} = 6$ and $N_{0\mathrm{Ch}} = 4$ for $E_{\mathrm{ref}} = 0$. In the presence of interactions U, the above point-gap closing does not occur. Therefore, one can identify the topology of $N_{0\mathrm{Ch}} = 6$ and that of $N_{0\mathrm{Ch}} = 4$ in the presence of interactions. Correspondingly the topology is characterized by ν which takes $\nu = 1$ in the entire region.

In the following, we numerically demonstrate that interactions allow the smooth deformation of $\hat{H}$ characterized by $N_{0\mathrm{Ch}} = 6$ to the $\hat{H}$ characterized by $N_{0\mathrm{Ch}} = 4$

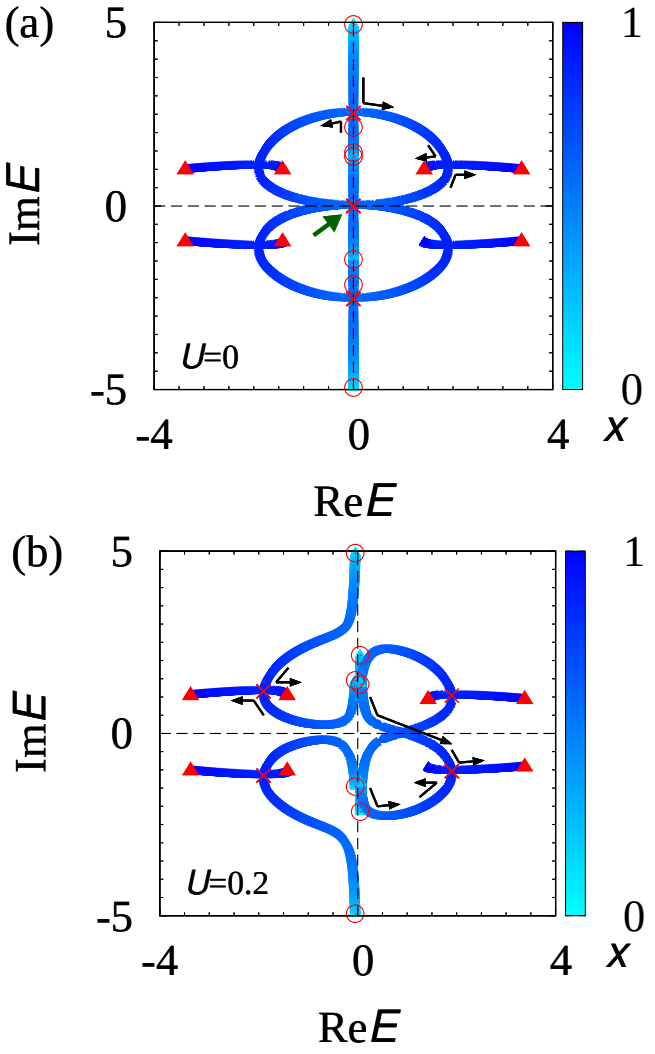

FIG. 10. (a) [(b)] Spectral flow of $\hat{H}_{(3,0)}$ for $U = 0$ [0.2]. With increasing x from 0 to 1, the eigenvalues flow along blue curves as indicated by black arrows. In panel (a) [(b)], eigenvalues for $x = 0$, 0.6, and 1 [$x = 0$, 0.8725, and 1] are denoted by open circles, crosses, and closed triangles, respectively. In panel (a), the point-gap at $E_{\mathrm{ref}} = 0$ closes as denoted by the green arrow. The flow in panel (a) is symmetric about the real- and imaginary-axes due to Eqs. (15) and (18a). The flow in panel (b) is symmetric about the real-axis due to Eqs. (15). These data are obtained for $(\beta, \gamma_1, \gamma_0, \gamma_{-1}) = (0.8, -3, -2.945, 1)$.

which keeps the point-gap and chiral symmetry. Figures 10(a) and 10(b) display the spectral flow for $U = 0$ and $U = 0.2$, respectively. As shown in Fig. 10(a), the point-gap closes at $x = x_c \sim 0.6$ in the non-interacting case [see also Fig. 11]. In contrast, the point-gap remains open in the interacting case [see Fig. 10(b)], which is consistent with the phase diagram [see Fig. 9].

In a similar way, we can see that the gap remains open along the path parameterized by λ ($0 \le \lambda \le 1$) which is illustrated by dashed arrows in Fig. 9. Figure 12 indicates that interactions allow the smooth deformation of

$\hat{H}$ characterized by $N_{0\mathrm{Ch}} = 6$ to the $\hat{H}$ characterized by $N_{0\mathrm{Ch}} = 4$ which keeps the point-gap and chiral symmetry.

The above results justifies the reduction of the point-gap topology $\mathbb{Z} \to \mathbb{Z}_2$ for zero-dimensional systems with chiral symmetry.

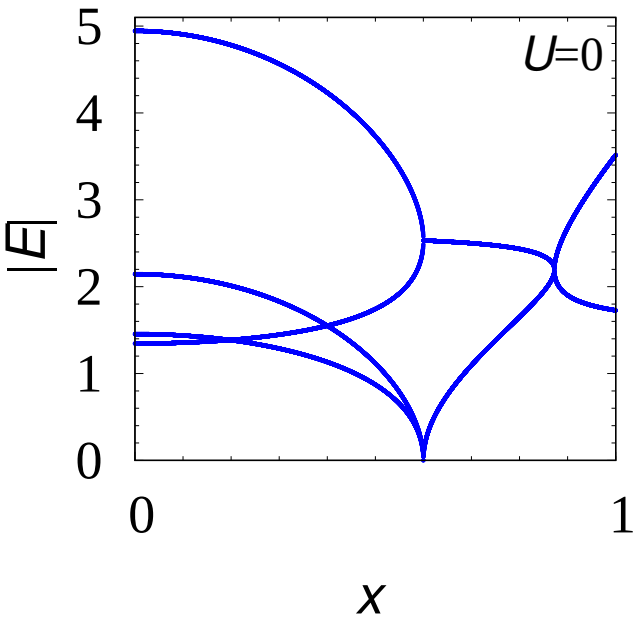

FIG. 11. The absolute value of eigenvalues $|E_n|$ $(n = 1, \ldots, 8)$ as functions of x for $U = 0$. At $x = x_c \sim 0.6$, the eigenvalues become zero.

The previous work[92] has also addressed the reduction phenomenon. We note, however, that Ref. 92 has compared the topology of the first-quantized Hamiltonian h and the second-quantized Hamiltonian $\hat{H}$. In contrast, the analysis provided in this section compares the topology of the non-interacting second-quantized Hamiltonian $\hat{H}_0$ with that of the interacting second-quantized Hamiltonian $\hat{H}$ which clearly elucidates that the $\mathbb{Z}$ group formed by the point-gap topological states in non-interacting cases reduces to its subgroup $\mathbb{Z}_2$ due to the interactions [see Eq. (23)].

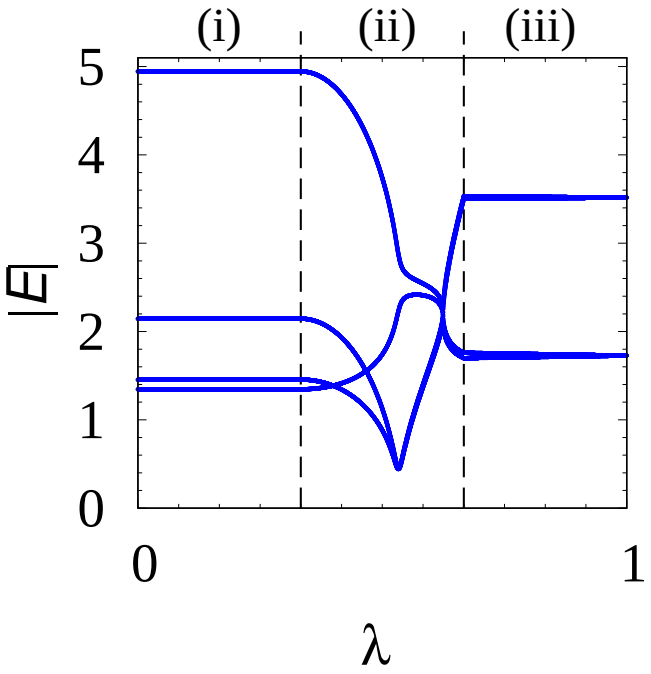

FIG. 12. The absolute value of eigenvalues $|E_n|$ $(n = 1, \ldots, 8)$ as functions of λ which parameterizes the path illustrated in Fig. 9. On the dashed vertical lines λ takes $\lambda = 1/3$ and $2/3$, respectively. Here, λ parameterizes (x, U) as follows: [region (i)] for $0 \leq \lambda < 1/3$, it parameterizes as $(x, U) = (0, 0.6\lambda)$; [region (ii)] for $1/3 \leq \lambda < 2/3$, it parameterizes as $(x, U) = (3\lambda - 1, 0.2)$; [region (iii)] $2/3 \leq \lambda \leq 1$, it parameterizes as $(x, U) = (1, 0.2 - 0.6\lambda)$.